

The multi-axial strength performance of composite structural B-C-W members subjected to shear forces

Limeng Zhu ^{1a}, Chunwei Zhang ^{*1}, Xiaoming Guan ^{1b}, Brian Uy ^{2c}, Li Sun ^{3d} and Baolin Wang ^{4e}

¹ School of Civil Engineering, Qingdao University of Technology, Qingdao 266033, P.R. China

² School of Civil Engineering, University of Sydney, Sydney, 2006, Australia

³ School of Civil Engineering, Shenyang Jianzhu University, Shenyang 110168, P.R. China

⁴ Graduate School at Shenzhen, Harbin Institute of Technology, Harbin 150001, P.R. China

(Received November 4, 2017, Revised January 31, 2018, Accepted February 2, 2018)

Abstract. This paper presents a new method to compute the shear strength of composited structural B-C-W members. These B-C-W members, defined as concrete-filled steel box beams, columns and shear walls, consist of a slender rectangular steel plate box filled with concrete and inserted steel plates connecting the two long-side steel plates. These structural elements are intended to be used in structural members of super-tall buildings and nuclear safety-related structures. The concrete confined by the steel plate acts to be in a multi-axial stressed state: therefore, its shear strength was calculated on the basis of a concrete's failure criterion model. The shear strength of the steel plates on the long sides of the structural element was computed using the von Mises plastic strength theory without taking into account the buckling of the steel plate. The spacing and strength of the inserted plates to induce plate yielding before buckling was determined using elastic plate theory. Therefore, a predictive method to compute the shear strength of composited structural B-C-W members without considering the shear span ratio was obtained. A coefficient considering the influence of the shear span ratio was introduced into the formula to compute the anti-lateral bearing capacity of composited structural B-C-W members. Comparisons were made between the numerical results and the test results along with this method to predict the anti-lateral bearing capacity of concrete-filled steel box walls. Nonlinear static analysis of concrete-filled steel box walls was also conducted by using ABAQUS and the results agreed well with the experimental data.

Keywords: shear strength; multi-axial stressing state; concrete failure criterion; shear span ratio; buckling; nonlinear static analysis

1. Introduction

Steel-concrete composite structures have been widely used in earthquake prone regions due to their high efficiency and reasonable economy of the steel and concrete materials (Wang *et al.* 2017a). The cross section of the structural elements could largely be decreased, which could save a big space and make buildings more slender. Composite columns and shear walls are the most important structural members in tall and super tall buildings because of their high carrying capacity and lateral stiffness (Pant *et al.* 2017). Several types of steel plate-concrete composite walls have been studied, which could be divided into three kinds according to the relative position of steel plates and concrete, named as steel plates encased in reinforced concrete (CSC walls), steel plates embedded in reinforced concrete frames (SIF walls) and exterior steel plates with

concrete infill (SCS walls) (Zhao and Astaneh-Asl 2004). CSC walls and SIF walls are frequently used in reinforcement design of frame structures against lateral loads. CSC walls could prevent the buckling of steel plates, but do not improve the performance of concrete and increase the construction complexity (Dastfan and Driver 2016). SIF walls can improve the shear buckling behavior of the steel plates effectively, but fail to carry the high axial loads (Wang *et al.* 2017b). SCS walls consist of two surface steel plates and core concrete, which can both improve the buckling behaviour of steel plates and the performance of the concrete (Liew *et al.* 2017). The existence of the steel plates replace the building template, which facilitates the energy conservation and environmental protection. Some innovative designs such as novel J-hook connectors, ultra-lightweight concrete, profiled steel plate, bolted connection and welded insert steel plate connections have been developed to enhance the seismic behavior of SCS walls. Many researchers have carried out experimental and FEM based study and found that this kind of composite wall is characterized by high strength and ductility. Bradford *et al.* (1998) and Uy *et al.* (2001) considered the service and ultimate load behavior of profiled composite walls. Clubley *et al.* (2003) developed several shear connection failure modes based on the push out tests and numerical analysis. Hossain and Wright (2004) conducted small-scale model tests on double skin composite element

*Corresponding author, Professor,
E-mail: zhangchunwei@qut.edu.cn

^a Ph.D., E-mail: zhulimeng@qut.edu.cn

^b Ph.D., E-mail: guanxiaoming@qut.edu.cn

^c Professor, E-mail: brian.uy@sydney.edu.au

^d Professor, E-mail: sunli@sjzu.edu.cn

^e Professor, E-mail: wangbl@hitsz.edu.cn

to describe their bending and deformation behaviour and developed analytical models for strength and stiffness. Link and Elwi (2004) conducted numerical and experimental research on the behaviour of CSC walls. Rahai and Hatami (2009), and (Vecchio and McQuade 2011) have carried out research on the cyclic loading behaviour of SCS walls and found that this kind of composite shear walls could bear high compressive forces and have high ductility. Chen *et al.* (2015), conducted cyclic loading tests of double steel plate–high strength concrete composite walls and investigated that their primary failure mode was axial–flexural mode characterized by local buckling of the steel plates. The research further explored that small ratio of tie bar spacing to steel plate’s thickness could enhance the deformation capacity. Rafiei *et al.* (2013, 2015) and Hossain *et al.* (2016a and b) conducted finite elemental analysis and tests for profiled composite walls to investigate their in-plane shear performance. The research demonstrated that the effective connection between the profiled steel plates could enhance their deformation ductility. Huang and Liew (2016a, b, c), developed a new form of J-hook connector to connect the external plates. Bending test and simulation results showed that the J-hook connector enhanced the combed resistance. Zhou *et al.* (2016) developed a bolted connection between the steel plates of SCS walls. The test results showed that the setting of more binding bars could improve the in-plane shear behavior effectively. The previous studies demonstrate the high performance of SCS walls, the connection between exterior steel plates being the key factor influencing their performance but does not propose a single method to describe the confining effect of core concrete.

Concrete-filled steel box walls (CFSB walls) belonging to SCS walls are defined herein as concrete-filled slender steel box walls with insert plate connecting the two long-side plates (Fig. 1) and characterized by high strength and significant deformation ductility for compressive and shear loading due to the strong connection between the exterior steel plates. The CFSB wall can serve as both a structural unit and a prefabricated construction system. Insert plates are used to connect the long-side steel plates. These insert plates enable composite action of the plates and concrete and serve to limit steel plate’s buckling. In addition, concrete confined by the steel plates is in multi-axial

compression and its shear capacity is significantly improved. Three $\frac{1}{4}$ -scaled specimens of CFSB walls were built to take cyclic shear loading test by Emori (2002). The shear test exhibited the high strength and significant ductility of CFSB walls. Welded connection was used between the insert plates and the long-side steel plate which would result in the deficiency of the steel plates and is difficult to be considered for engineering applications. The information on the shear test has been documented in the research described by Emori (2002). Based on the findings of Emori (2002), a study on the shear strength of CFSB walls has been carried out.

The shear effect of the long-side steel plates and concrete of CFSP walls is obvious. The objective of this study is firstly, to obtain a method to clearly model the composite action and to calculate the shear strength of CFSB walls on the basis of multi-axial concrete strength theory. Secondly, on the basis of FEM analysis results, a reduction coefficient will be deduced to improve this method to compute the ultimate anti-lateral bearing capacity of CFSB walls with different shear span ratios. This research did not consider the influence of X-directional thickness which was used to calculate the aspect ratio of cross section to distinguish the differences between columns and walls. The influence of axial forces was investigated as one parameter in this study. Therefore, this proposed method can also be used to calculate the anti-lateral bearing capacity of concrete-filled steel box columns and beams subjected to shear forces, which could describe the multi-axial strengthening performance of composite structural B-C-W members when being subjected shear forces.

2. Shear strength of composite structural B-C-W members

2.1 Five assumptions

In order to analyze the typical shear behavior of composite structural B-C-W members and to obtain their shear strength, one structural element of CFSB walls has been chosen. The coordinate system has been shown in Fig. 2. Five assumptions were made for the chosen structural

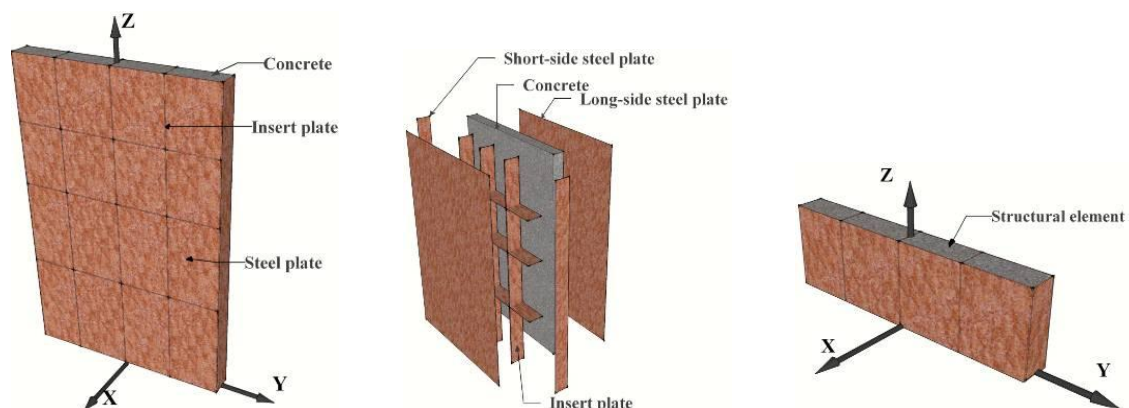


Fig. 1 Concrete-filled steel box walls and the coordinate system

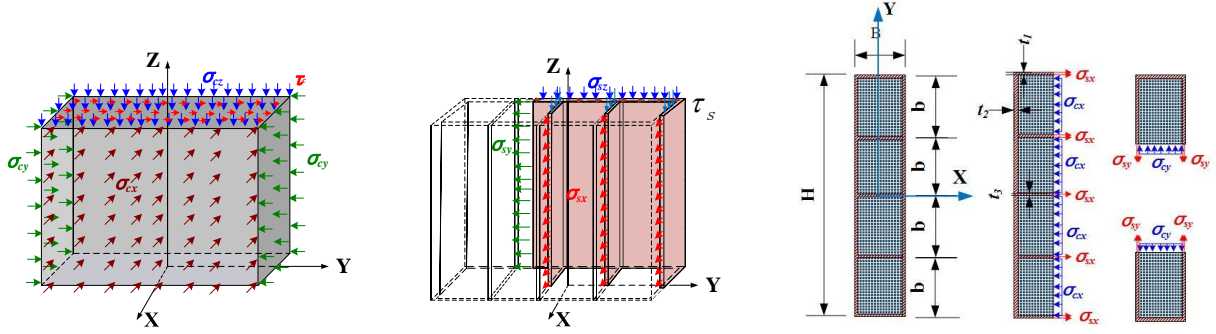


Fig. 2 The confinement stress of core concrete

element. Following are the assumptions:

- (1) The steel plates and insert plates yield when the CFSB wall attains its bearing capacity.
- (2) The X-direction normal stress (σ_{cx}) in the core concrete restrained by the steel plate is uniformly distributed (Fig. 2).
- (3) The structural elements of SCS walls are assumed to come into shear-failure mode. The long-side steel plates and concrete are assumed to consider the evenly distributed normal stress. The shear stress (τ_c) of the core concrete and the shear stress (τ_s) of the long-side steel plate in the XY plane are assumed to be uniformly distributed (Fig. 2).
- (4) The CFSP wall is presumed to be elastic when bearing the axial compressive force. Therefore, the Z-axial stress of long-side steel plates, short-side steel plates, insert plates (σ_{sz}) and the core concrete (σ_{cz}) can be calculated using elastic material models. Where σ_{cz} refers to the normal stress of concrete in Z direction.

The slip deformation between the core concrete and steel plate has not been considered.

2.2 Shear strength of core concrete

Because of the binding effects, the core concrete is in

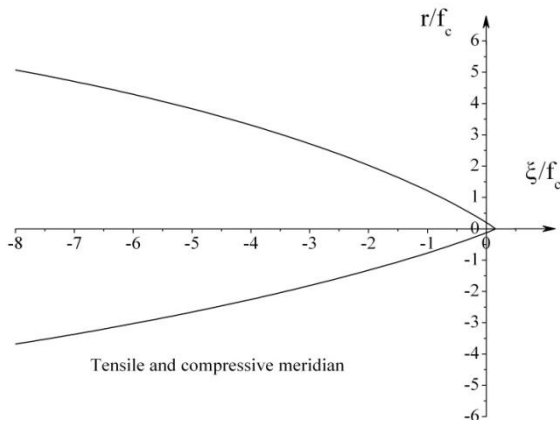
multi-axial stress state and its shear strength is eventually improved. The Guo- Wang (Guo and Wang 1991) concrete failure criterion was used in this study to calculate the concrete shear strength in multi-axial stress state. This failure criterion of the concrete has been described in Eqs. (1) and (2)

$$\frac{\tau_{oct}}{f_c} = a \left(\frac{b - \sigma_{oct}/f_c}{c - \sigma_{oct}/f_c} \right)^d \quad (1)$$

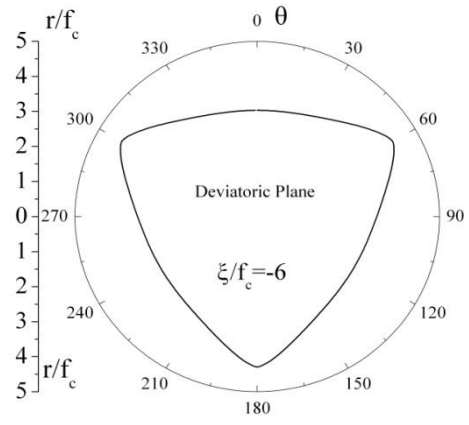
$$c = c_t \left(\cos \frac{3}{2} \theta \right)^{1.5} + c_c \left(\sin \frac{3}{2} \theta \right)^2 \quad (2)$$

In the above equations, σ_{oct} is the octahedral normal stress; τ_{oct} is the octahedral shear stress; θ is lode angle; f_c is uni-axial compression strength; and the coefficients are $a = 0.9638$; $b = 0.09$; $c_t = 12.2445$; $c_c = 7.3319$; $d = 0.9297$; $\sigma_{oct} = (\sigma_1 + \sigma_2 + \sigma_3) / 3$; $\tau_{oct} = \frac{\sqrt{(\sigma_1 - \sigma_2)^2 + (\sigma_2 - \sigma_3)^2 + (\sigma_3 - \sigma_1)^2}}{3}$; $\theta = \arccos \left[\frac{(2\sigma_1 - \sigma_2 - \sigma_3)}{(3\sqrt{2}\tau_{oct})} \right]$.

According to the coefficients above, the Guo-Wang concrete failure surface can be calculated. Its tensile and compressive meridian lines have been shown in Fig. 3(a) and its deviatoric plane ($\xi/f_c = 6$) has been illustrated in Fig. 3(b). In Fig. 3, $\xi = \frac{\sigma_1 + \sigma_2 + \sigma_3}{\sqrt{3}}$; $r = \frac{\sqrt{(\sigma_1 - \sigma_2)^2 + (\sigma_2 - \sigma_3)^2 + (\sigma_3 - \sigma_1)^2}}{3}$; $\cos \theta = \frac{(2\sigma_1 - \sigma_2 - \sigma_3)}{(\sqrt{6}r)}$; $\sigma_1, \sigma_2, \sigma_3$

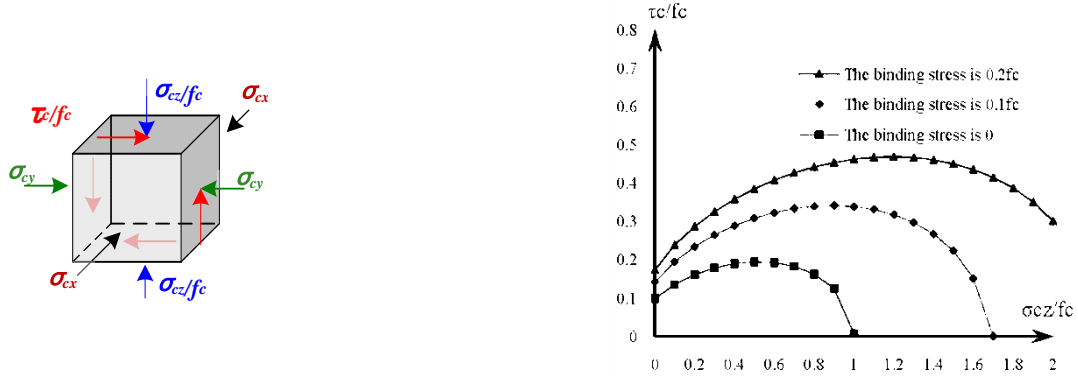


(a) The tensile and compressive meridian lines



(b) The deviatoric plane

Fig. 3 Guo-Wang concrete failure surface

(a) The assumed stress state of concrete ($\sigma_{cx} = \sigma_{cy}$)

(b) The calculated results using Guo-Wang concrete failure criterion

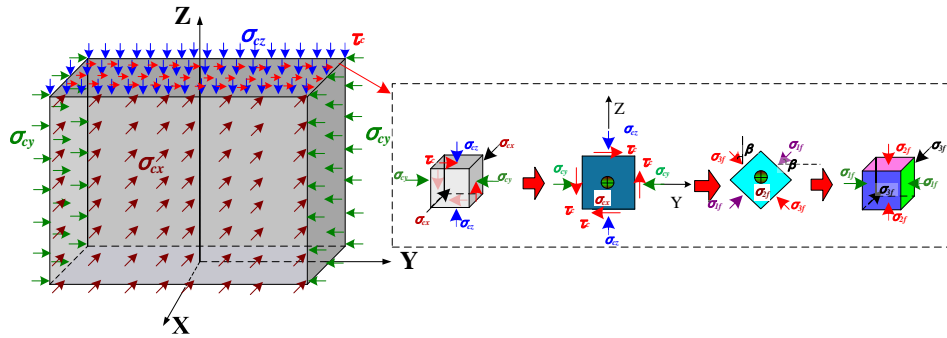
Fig. 4 The shear strength of concrete under different confining stress and axial stress ($\sigma_{cx} = \sigma_{cy}$)

Fig. 5 The principle stress of the core concrete

are the principle stresses ($\sigma_1 > \sigma_2 > \sigma_3$). The compressive stress is positive and the tensile stress is negative.

The concrete is assumed to be in multi-axial stress state as shown in Fig. 4(a) and normal stress of concrete in X direction (σ_{cx}) is equal to normal stress of concrete in Y direction (σ_{cy}) which is the binding stress changing from $0.1f_c$ to $0.2f_c$. Under the same binding stress level, the normal stress of concrete in Z direction (σ_{cz}) increases gradually and the corresponding shear strength of concrete (τ_c) can be calculated as illustrated in Fig. 4(b).

When the confining stress was zero, the shear strength of the concrete (τ_c) increased with the increment of normal stress of concrete in Z direction (σ_{cz}) until σ_{cz} / f_c reached 0.5. Then, τ_c decreased and when σ_{cz} / f_c reached 1.0, it became zero. When the confining stress was in the interval between $0.1f_c$ and $0.2f_c$, typical for shear walls of the buildings, both of the shear strength and the axial strength of concrete increased with the increase of the confining stress as expected (Fig. 4). Therefore, the Guo-Wang concrete failure criterion has been adopted in this research.

The Z-direction axial stress in the steel plate (σ_{sz}) and the core concrete (σ_{cz}) was computed using an elastic model. The axial stress along the short-side steel plate and the insert plate in X-direction (σ_{sx}) was calculated using Von Mises strength criterion. The axial stress of the long-side steel plate in Y-direction σ_{sy} varied ($0.1f_y, 0.2f_y, \dots$). The confining stresses (σ_{cx}, σ_{cy}) in core concrete were computed accordingly. Three principal stresses (Eqs. (3)-(5), Fig. 5) of the core concrete were obtained as a function of the shear

strength of concrete (τ_c).

$$\sigma_1 = -\frac{\sigma_{cy} + \sigma_{cz}}{2} + \sqrt{\frac{(\sigma_{cy} - \sigma_{cz})^2}{4} + \tau_c^2} \quad (3)$$

$$\sigma_3 = -\frac{\sigma_{cy} + \sigma_{cz}}{2} - \sqrt{\frac{(\sigma_{cy} - \sigma_{cz})^2}{4} + \tau_c^2} \quad (4)$$

$$\sigma_2 = -\sigma_{cx} \quad (5)$$

A single equation was obtained when the three principal stresses calculated by Eqs. (3)-(5) were substituted into the Guo-Wang concrete failure criterion (Eqs. (1)-(2)) while the shear strength of concrete was computed iteratively.

2.3 Limit value of the steel plate slenderness

Liang *et al.* (2003, 2004) proposed the local buckling models for steel plates in double skin composite panels (DSC) which include shear and biaxial compression with corresponding initial imperfections. Steel plates in DSC panels were restricted to buckle locally between shear studs and models with various boundary conditions were proposed to simulate their buckling behavior. Design models were proposed for calculating the maximum stud spacing and the ultimate strength of steel plates in DSC panels.

Buckling strength of the steel plate was significantly

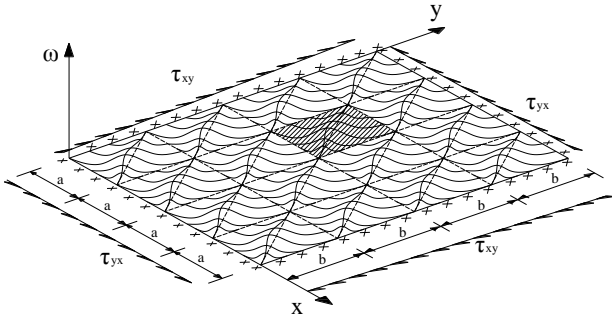


Fig. 6 The buckling model of the long-side plate

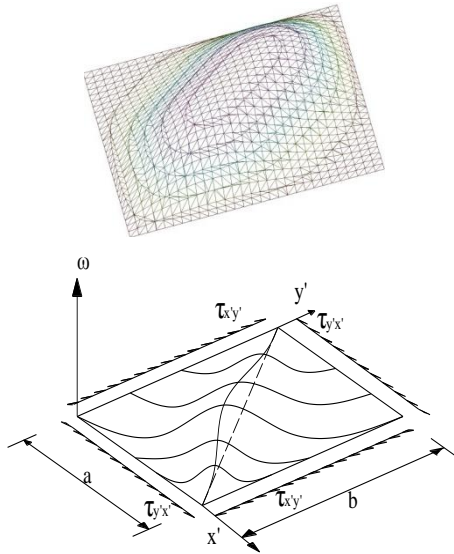


Fig. 7 The unit for calculating the elastic buckling stress

increased due to the supporting effect of the concrete and existence of inserted plates. Because of the existence of inserted steel plates which were welded to the long-side steel plates, clamped boundary conditions have been proposed for square steel plates to analyze their buckling behavior. This clamped boundary condition given by the inserted plates is more helpful in improving the local buckling behavior than that of the shear stud connectors in DSC panel. Therefore, the maximum inserted steel plate spacing of composite structural B-C-W members is much larger than the maximum shear stud spacing of shear walls using shear stud connectors.

Elastic plate theory was utilized to calculate the appropriate spacing of insert plates to make the steel plate yield before buckling. The buckling model of the steel plate in Fig. 6 shows the composite structural B-C-W members under shear force. One unit area (Fig. 7) was chosen to analyze the buckling stress. Eq. (6) describes the clamped boundary conditions and Eq. (7) refers to the buckling displacement.

$$\left. \begin{aligned} x=0, x=a, \omega = \frac{\partial \omega}{\partial x} = 0; \\ y=0, y=b, \omega = \frac{\partial \omega}{\partial y} = 0 \end{aligned} \right\} \quad (6)$$

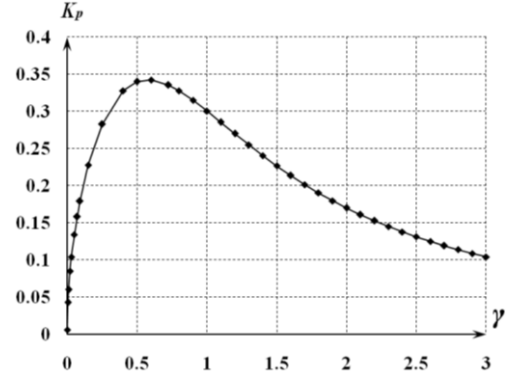


Fig. 8 The γ - K_p relationship curve

$$\omega = \frac{f}{2} \sin\left(\frac{\pi x'}{a}\right) \cdot \sin\left(\frac{\pi y'}{b}\right) \cdot \left(1 - \cos\frac{\pi x'}{a} \cdot \cos\frac{\pi y'}{b}\right) \quad (7)$$

In these equations, f is the maximum displacement; a is the spacing of insert plate in X-direction and b is the spacing of insert plates in Y-direction.

The spacing of insert plates in X and Y directions were known; the elastic buckling stress of the steel plate was derived using Eq. (8)

$$\left. \begin{aligned} \tau_{cr} &= \frac{\pi^2 E}{12(1-\nu^2) \cdot (K_p \cdot b/t)^2} \\ K_p &= 1/\sqrt{\gamma \cdot (2.77\gamma^2 + 2.77/\gamma^2 + 5.54)}; \gamma = b/a \end{aligned} \right\} \quad (8)$$

Where, σ_{cr} is the elastic buckling stress of the steel plate; $E = 2 \times 10^5$; $\nu = 0.3$; b/t is the steel plate slenderness and K_p is the buckling length coefficient. γ is the ratio of spacing of insert plates in X and Y directions.

According to Eq. (8) the γ - K_p relationship curve was obtained as shown in Fig. 8. The buckling length coefficient K_p reached its maximum value when γ was 0.725.

The spacing of insert plates in X and Y directions were assumed equal. The limit value of the steel plate slenderness b/t was attained when the elastic buckling stress of the steel plate became equal to the yield stress ($f_y = 235$ MP). The theoretical value of K_p was taken as 0.305. In case of an SCS wall under moment and shear force, tensile deformation occurred on insert plates and buckling shape appeared only on one segment between the binding bars. The initial imperfection of the steel plate was not considered in the analysis. Therefore, the standard buckling length coefficient should be greater than 0.305 and the suggested design value is 0.5.

The elastic buckling stress was larger than the yield stress when the steel plate slenderness was less than 73 (Fig. 9). Therefore, the limit value of the spacing of insert plates was deduced.

2.4 Shear strength of the steel plate

The Z-direction steel plate's axial stress (σ_{sz}) was computed as above. Because of the supporting effect of the core concrete and insert plates, buckling of the steel plate

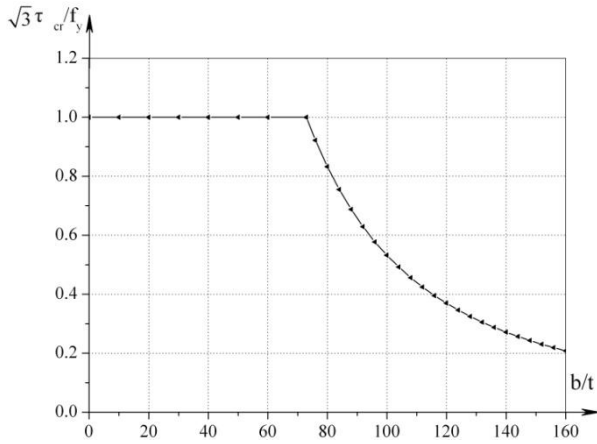


Fig. 9 The elastic buckling stress – steel plate slenderness relationship curve ($K_p = 0.5$)

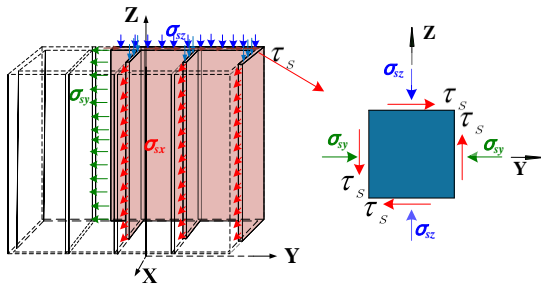


Fig. 10 The stress of the steel plate

was avoided. Therefore, the von Mises strength theory (Eq.(9)) was applied to compute the shear strength (τ_s) of the long-side steel plate. Fig. 10 shows the stress state of steel plates.

$$\tau_s = \sqrt{\frac{f_y^2 - (\sigma_{sy}^2 + \sigma_{sz}^2 + \sigma_{sy}\sigma_{sz})}{3}} \quad (9)$$

Where, f_y = the yielding stress of the steel plate.

2.5 Methods to obtain the shear strength of composite structural B-C-W members

The shear strength of core concrete and the shear strength of long-side steel plate was computed through the above calculations and as a result a predictive equation (Eq. (10)) was developed to calculate the shear strength of the SCS walls. The predictive equation was developed by adding the shear strengths of core concrete and the long-side steel plate

$$V_c = \tau_c A_c + \tau_s A_{sl} \quad (10)$$

where A_c = the area of the core concrete, A_{sl} = the area of the long-side steel plate, V_c is the shear strength of the cross section. The steps to calculate the shear strength of SCS walls have been presented in Fig. 11.

The described method was used to calculate the shear strength of SCS walls, which also could be used for

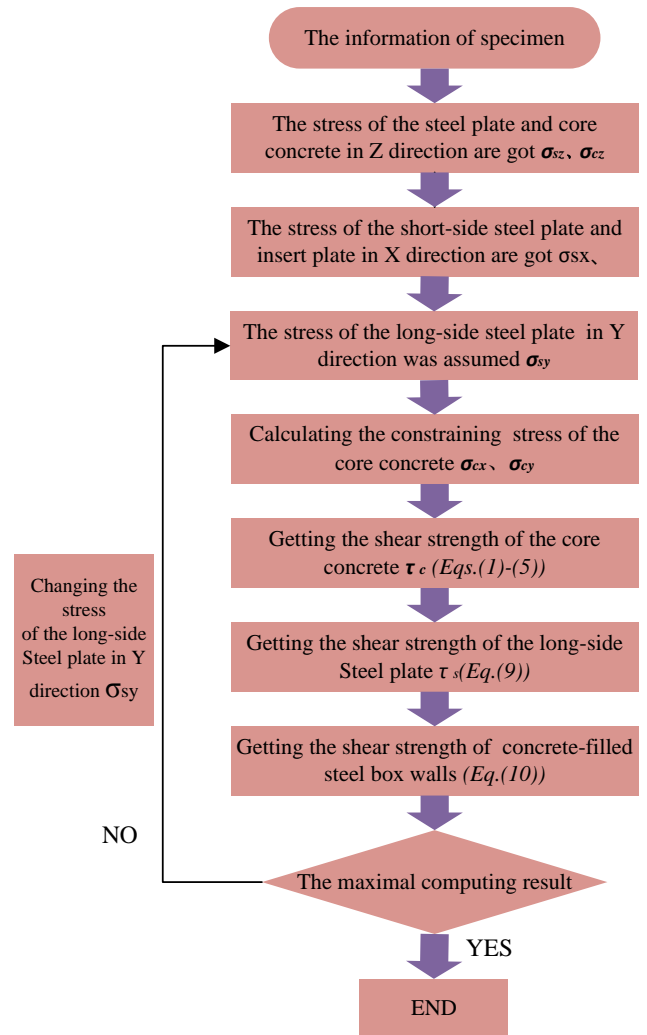


Fig. 11 The steps of calculating shear strength of SCS walls

concrete-filled steel box beams and columns in the same boundary conditions. Based on the multi-axial strength theory, the shear strength of SCS walls can be computed. However, it wasn't successful in computing the influence of the shear span ratio. Therefore, strength reduction coefficient was required and it was computed to fit the experimental data from the test done by Emori (2002) and the finite element results.

3. Comparison with the experimental data

The experimental data was cited from the shear loading test of concrete-filled box walls (Fig. 13) carried out by Emori (2002). Three types of testing specimens with surface steel plate's width-thickness ratios of 200 ($= b/t = 640 \text{ mm}/3.2 \text{ mm}$), 100 ($= b/t = 320 \text{ mm}/3.2 \text{ mm}$) and 67 ($= b/t = 216/3.2$) were used in this research. These specimens were named as 200K, 100K and 67K, respectively. The shear loading test specimens were subjected to both bending and shear force, simulating the fixed constrains at the two ends as shown in Fig. 12. The middle part of specimen 67K

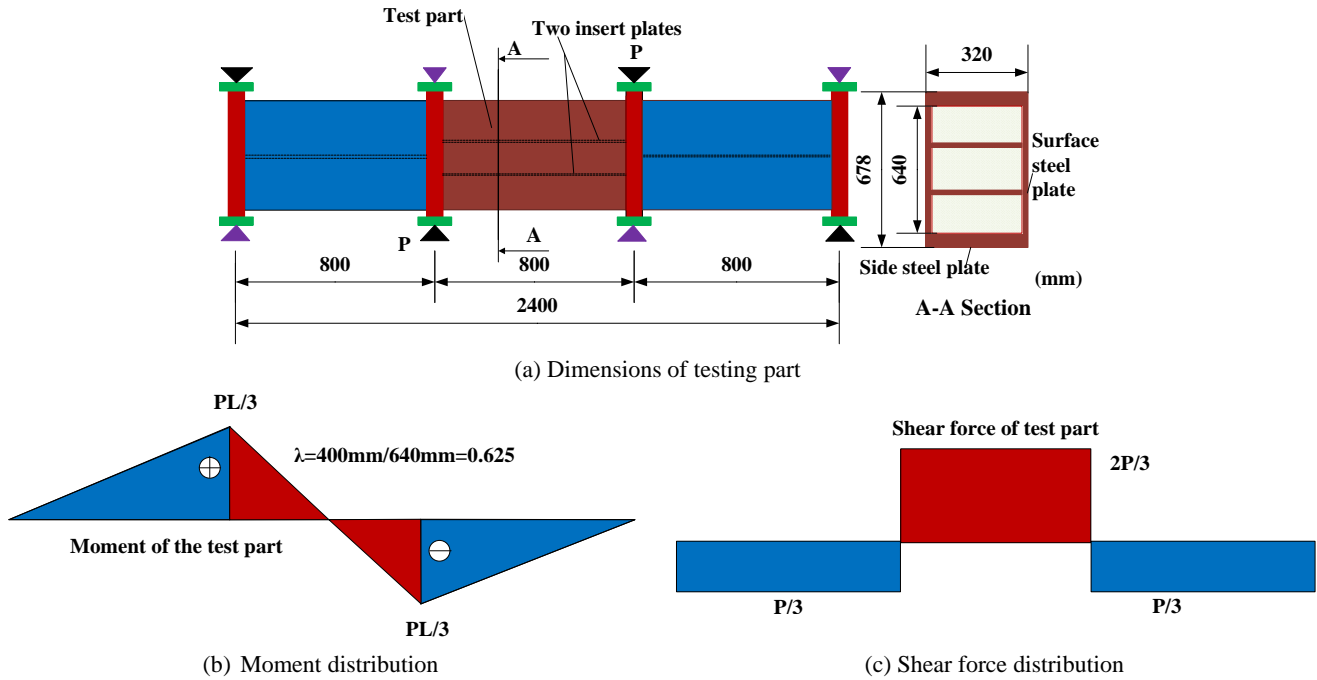


Fig. 12 Details of shear test specimen 67K

is the shear testing part and its shear force is $2P/3$ where P is the loading force in the loading point. The considered dimensions of the SCS wall unit for the test are 640 mm width by 800 mm high by 320 mm.

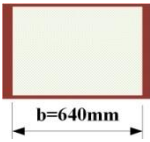
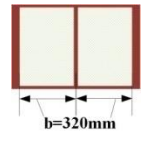
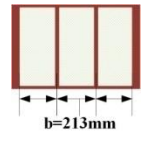
The parameters related to the specimen's experimental and numerical results have been illustrated in Table 1. The thickness of the long-side steel plate and insert steel plate was 3.2 mm while thickness of short-side steel plate was 19 mm. The strength of the concrete was 23.4 N/mm^2 and the yielding stress of the steel was 253 N/mm^2 . Tensile strength of steel was 402 N/mm^2 , the cross section of the specimen was $640 \text{ mm} \times 320 \text{ mm}$ and the shear span ratio of specimens were 0.625 ($\lambda = 0.625$). The strengthening design of side steel plates is to prevent flexural failure of the SCS

wall unit and to make the shear effects of surface steel plates and concrete more obvious. Under this special design situation, the side steel plates bear more bending moment, decreasing the moment that the surface steel plate bears simultaneously. The shear behavior of surface steel plates and concrete become more obvious than that of traditional columns. The shear effect of the surface steel plates and concrete is obvious, and under these conditions a method to describe their shear performance and mutual strengthening interactions has been proposed.

Where, b is the width of the cross section and t is the thickness of surface steel plates.

The shear strength of SCS walls (V_c) was computed using the above mentioned method without taking into

Table 1 Comparison with the experimental data

Specimen	Cross section	Width thickness ratio (b/t)	Number of insert plates (n)	Test V_t [MN]	Theory V_c [MN]
200K	 $b=640\text{mm}$	200	0	1.97	1.559
100K	 $b=320\text{mm}$	100	1	2.04	1.572
67K	 $b=213\text{mm}$	67	2	2.00	1.584

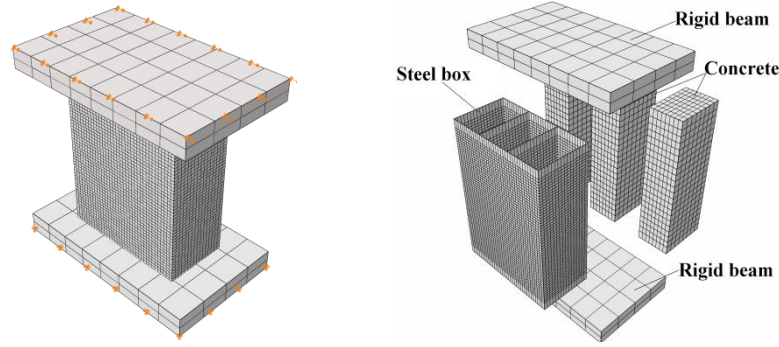


Fig. 13 Finite element model of specimen 67K

account the influence of shear span ratio. The theoretical results (V_c) were less than the test results (V_t). The shear strength of specimen computed based on the strength, increases with the number of the insert plate which is in consent with the shear test results.

4. Finite element method analysis

2-dimensional nonlinear FEM analysis was done by Emori (2002), but this model did not consider the influence of the initial imperfection of the steel plates and therefore, could not simulate the binding effect of the core concrete.

Shear test specimens 200K, 100K and 67K were carried out using 3-dimensional nonlinear FEM analysis in ABAQUS which took into account the contact and frictional effects between the concrete and steel plate. The objective of the FEM analysis is to obtain the available model of the SCS wall units to simulate the inelastic behavior of the steel box and concrete. Based on the defined finite element model, a parametric analysis study of SCS wall box units was made to obtain a strength reduction coefficient and to compute the horizontal capacity of SCS walls.

4.1 Analytical conditions

The steel box of shear test specimen 67K was divided into three 400 mesh elements and the insert plate was divided into 800 mesh elements as shown in Fig. 13. Each mesh element was modeled as a four-node doubly curved shell element with reduced integration S4R shell element. The core concrete was divided into three parts by the insert plates and each part was divided into 200 mesh elements. Each mesh element was modeled by an eight-node linear brick element C3D8 as shown in Fig. 13. Two ends of the specimen were embedded into the rigid beam to simulate the fixed constraint condition. A surface-to-surface contact was defined between the steel and concrete. The penalty method that permits some relative motion of the surfaces when they should be sticking was selected to simulate the tangential and normal behavior between the concrete and steel. The friction coefficient was taken as 0.6 (Rabbat and Russell 1985). The parameter setting of the finite element model of specimen 100K and 200K was the same as that of specimen 67K, except the geometric differences between

Table 2 Damaged plasticity model

Yielding function		Plastic potential function
$\sigma_1 \leq 0$	$f = q - 3ap + \gamma\sigma_1 - (1 - \alpha)\sigma_c = 0$	$g = q - p \tan\psi$
$\sigma_1 > 0$	$f = q - 3ap + \beta\sigma_1 - (1 - \alpha)\sigma_c = 0$	

them. For specimen 200K, there were no inserted steel plates and the concrete was not divided. For specimen 100K, there was one inserted steel plate and the concrete was divided into two parts.

The model of the steel and concrete used in the FEM analysis are as follows:

(1) The damaged plasticity model (Table 2) was used for concrete. Its failure surface has been illustrated in Fig. 15. The dilation angle of the concrete was 35° . The uniaxial compressive stress-strain curve of concrete (Eq. (11)) proposed by Guo and Wang (1991) was used in this analysis. The ascending part of the tensile stress-strain curve of the concrete was linear and the descending part of the curve was proposed by Guo and Wang (1991) (Eq. (12)).

$$\left. \begin{aligned} y_c &= \alpha_a x_c + (3 - 2\alpha_a)x_c^2 + (\alpha_a - 2)x_c^3, (0 \leq x_c \leq 1) \\ y_c &= x_c / [\alpha_d (x - 1)^2 + x_c], (x_c > 1) \end{aligned} \right\} \quad (11)$$

Where, $x_c = \varepsilon_c / \varepsilon_{c0}$, $y_c = \sigma_c / f_c$, $\varepsilon_{c0} = (700 + 172\sqrt{f_c}) \times 10^{-6}$, $\alpha_a = 2.4 - 0.0125f_c$, $\alpha_d = 0.157f_c^{0.785} - 0.905$.

f_c is the uni-axial compressive strength of the concrete, ε_{c0} is the peak compressive strain of the concrete, α_a , α_d are the parameters of the stress-strain curve.

$$\left. \begin{aligned} y_t &= x_t, \quad (0 \leq x_t \leq 1) \\ y_t &= x_t / [\alpha_t (x - 1)^{1.7} + x_t], (x_t > 1) \end{aligned} \right\} \quad (12)$$

Where, $x_t = \varepsilon_t / \varepsilon_{t0}$, $y_t = \sigma_t / f_t$, $\varepsilon_{t0} = 65 \times 10^{-6} f_t^{0.54}$, $\alpha_t = 0.312 f_t^2$, f_t is the tensile strength of the concrete, ε_{t0} is the peak tensile strain, α_t is a parameter of the tensile stress-strain curve.

Where, $p = -(\sigma_1 + \sigma_2 + \sigma_3) / 3$, $q = \frac{\sqrt{(\sigma_1 - \sigma_2)^2 + (\sigma_2 - \sigma_3)^2 + (\sigma_3 - \sigma_1)^2}}{2}$, $\cos \theta = (-2\sigma_1 + \sigma_2 + \sigma_3) / 2q$.

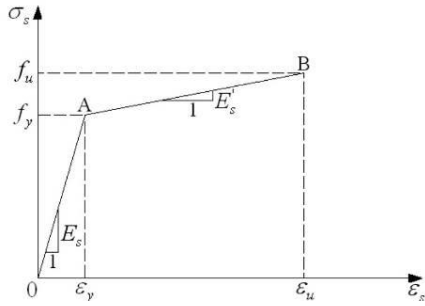


Fig. 14 Uniaxial tensile stress-strain curve of steel

α, β, γ are material parameters and ψ is the dilation angle.

The constitutive rule for the steel was based on the plasticity theory with the Von Mises (1928) yielding condition, which was also used in ACI 352R-02(2002). The stress-strain relationship for the steel box and insert plate was simply assumed as bi-linear model as shown in Fig. 14.

The strain hardening effect was considered in this model. The elastic modulus of steel before yielding was 206,000 N/mm² and the elastic modulus of steel after yielding was 4, 120 N/mm² as shown in Fig. 14. The

dilatancy effect of concrete caused the bulging of the steel box which eventually led to the buckling of the steel plate. Afterwards, the buckling was taken to be constant with respect to direction and magnitude.

The finite element model was built used to make a simple linear modal analysis mainly to investigate the buckling behavior of the surface steel plates without infill concrete. Therefore, in this finite element model, the contact between the concrete and steel plate was not defined. The modal analysis results have been shown in Figs. 15-17 which explain the influence of width-thickness ratio on the mutual strengthening interaction between steel plates and concrete.

The first buckling mode of specimen 200K has been shown in Fig. 15(a). The convex buckling occurred on both the two surfaces of the steel plates. Therefore, the existence of infilled concrete could not improve the buckling in mode-1 and the corresponding buckling stress of surface steel plates. But the infilled concrete could improve the buckling stress of surface steel plates in buckling mode-2 and mode-3, avoiding the concave buckling behavior of surface steel plates.

The buckling mode-1, mode-2 and mode-3 of specimen 100K have been shown in Fig. 16. It can be observed that

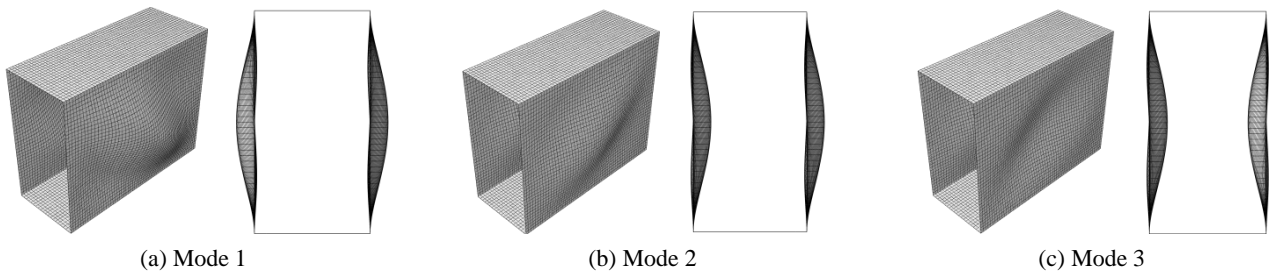


Fig. 15 The first three buckling modes of the steel box for specimen 200K

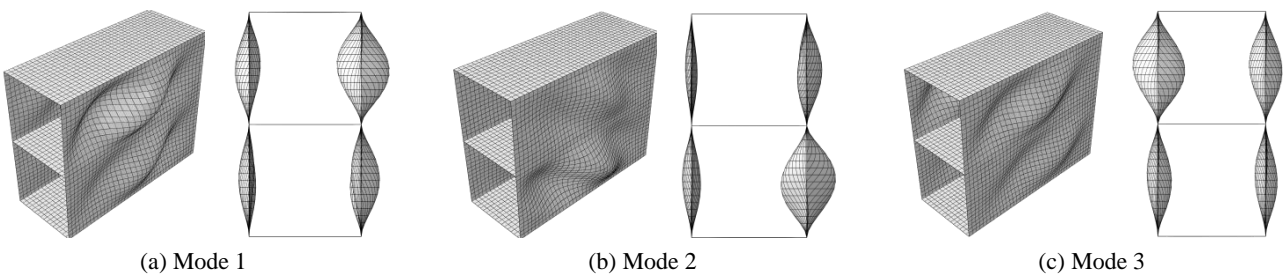


Fig. 16 The first three buckling modes of the steel box for specimen 100K

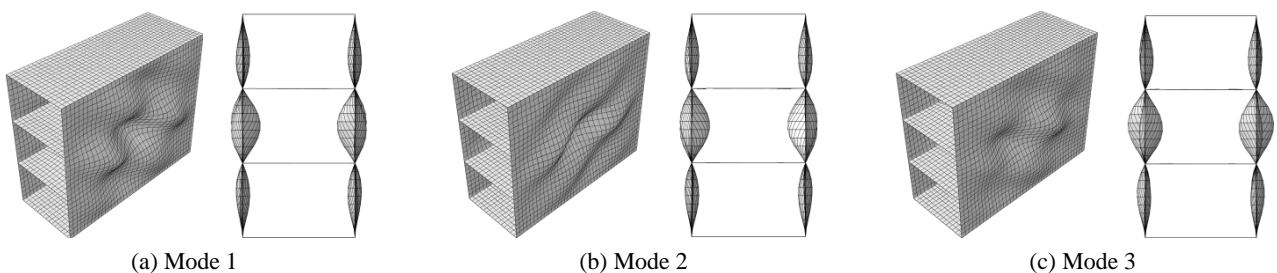


Fig. 17 The first three buckling modes of the steel box for specimen 67K

concave buckling happened on both the two surfaces of the steel plates. Therefore, it can be said that the existence of infilled concrete could improve the buckling stresses of surface steel plates corresponding to these three modes.

The buckling mode-1, mode-2 and mode-3 of specimen 67K have been shown in Fig. 17. The concave buckling occurred on both the two surfaces of the steel plates. Therefore, it can be said that the existence of infilled concrete could improve the buckling stresses of surface steel plates corresponding to these three modes.

Based on the above described analysis, it has been concluded that large width-thickness ratio of surface steel plates doesn't lead to the improved buckling behavior of steel plates. However, inserted steel plates could improve their mutual interaction.

4.2 Results of analysis

Fig. 18 shows the load-displacement envelope curves obtained from the shear test (Emori 2002) and Finite

element software ABAQUS. The computed load-displacement envelope curves are in close agreement to those obtained by shear test of the 67K specimen and 100K specimen up to ultimate strength. The computed load-displacement envelope curve agreed well with the results achieved by shear test of 200K specimen up to 5mm deflection. The computed results were smaller than the test results for 200K specimen, once a deflection of 5mm occurred.

Fig. 19 shows the concrete cracks, yield patterns and priciple stresses for the specimens (200K at $V_t = 1.81$ MN, 100K at $V_t = 1.72$ MN and 67K at $V_t = 1.72$ MN) obtained by the FEM analysis. The analyzed results agreed well with the test results which were discribed by Emori (2002) in the shear test.

A finite element model in ABAQUS was established and parametric analyses were carried out. Therefore, several models with different shear span ratios were made in ABAQUS in order to obtain a strength reduction coefficient to improve the method of computing the shear strength of

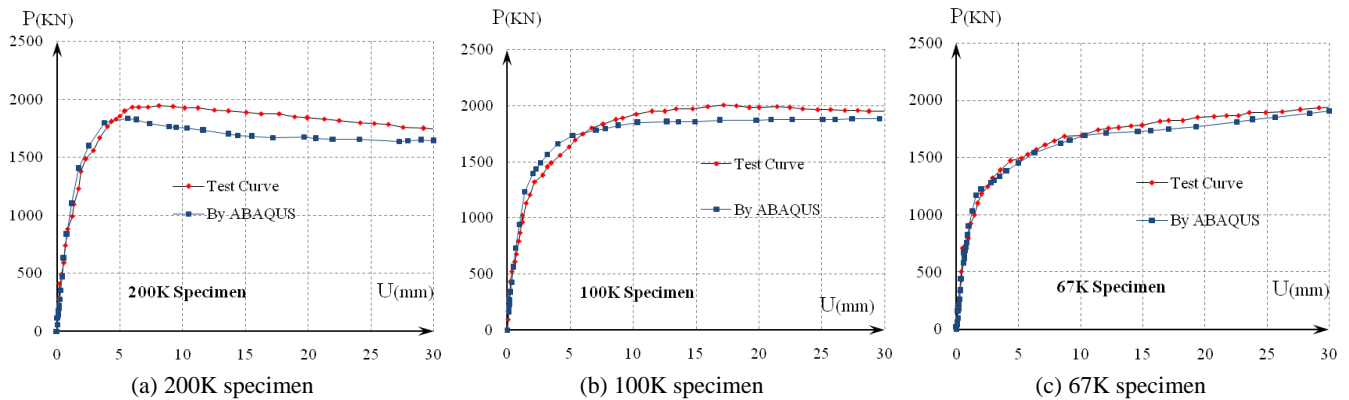


Fig. 15 The first three buckling modes of the steel box for specimen 200K

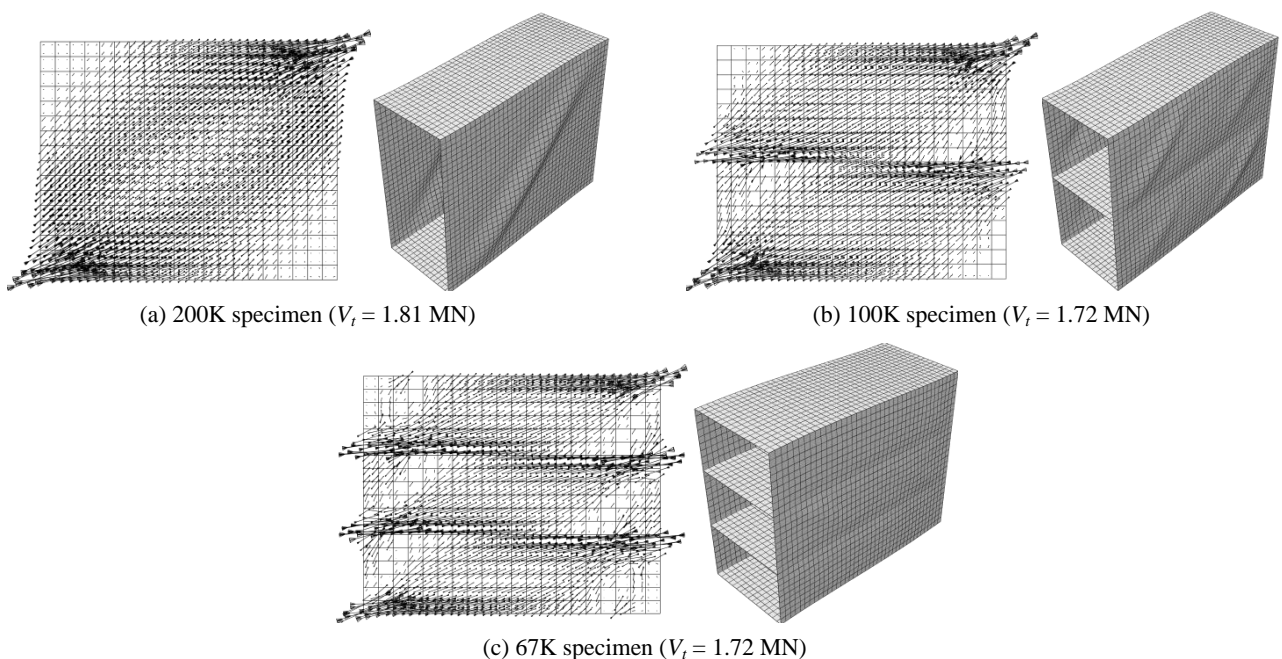


Fig. 19 The principal stresses of the concrete and deformation of the steel box for specimens

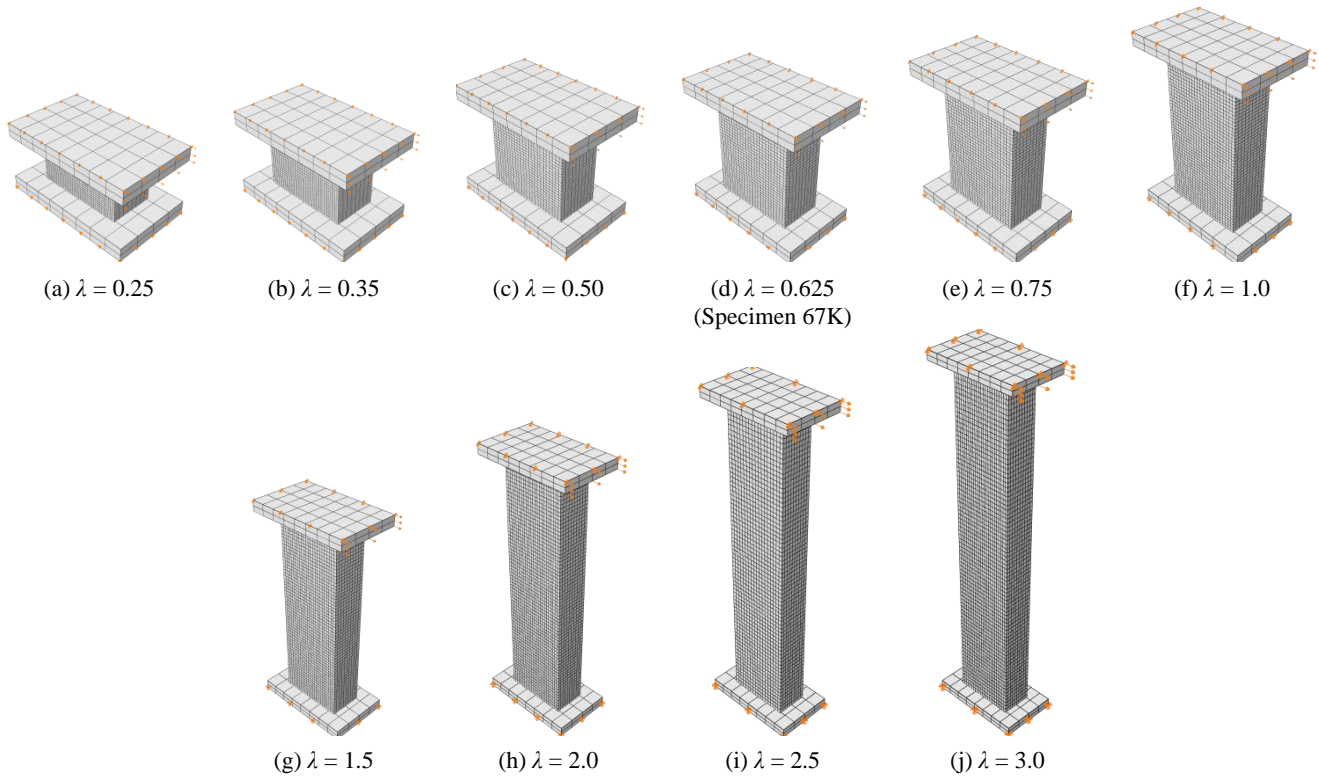


Fig. 20 Ten finite element models of SCS walls with different shear span ratios

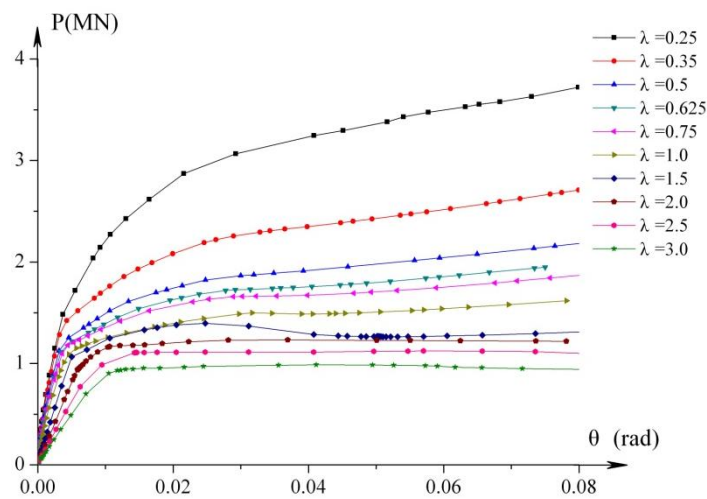


Fig. 21 Load-displacement envelope curves of SCS walls with different shear span ratios

concrete-filled steel box walls.

5. Ultimate anti-lateral bearing capacity of SCS walls with different shear span ratios

5.1 The coefficient with the shear span ratio

Based on the above analysis, a reasonable 3-dimensional finite element model was built and a set of ten finite element models with different shear span ratios were simulated in ABAQUS (Fig. 20).

Parameters besides the shear span ratio of these models

were the same as the FE model of 67K specimen. When the angular displacement reached 8/100, the SCS wall achieved its ultimate shear strength in the shear test of 67K specimen. Therefore, when the angular displacements of these models reached 8/100, the SCS walls resulted in a failure. The ultimate shear strength of SCS walls could be found in the computed load-displacement envelope curves as shown in Fig. 21.

The computed anti-lateral bearing capacity of ten finite element models have been presented in Table 3. The ultimate shear strength relationship curve has been shown in Fig. 22. According to the computed ultimate shear strength of SCS walls in ABAQUS, Eq. (13) was obtained to

Table 3 The ultimate shear strength of SCS walls with different shear span ratios using FEM method and multi-axial strength theory

Shear span ratio	FEM results [MN]	Theory V_{sc} [MN]
0.25	3.65	3.13
0.35	2.80	2.65
0.50	2.13	2.22
0.625	2.00	1.99
0.75	1.85	1.838
1.00	1.62	1.60
1.50	1.39	1.33
2.00	1.20	1.18
2.50	1.11	1.09
3.00	0.97	1.01

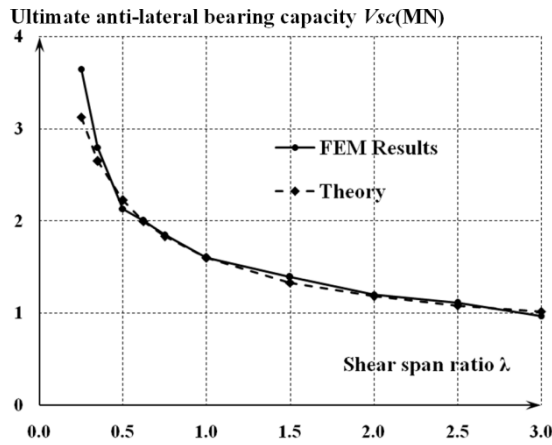


Fig. 22 Shear span ratio-ultimate anti-lateral bearing capacity curves of SCS walls using FEM method and multianxial strength theory

compute the influence of shear span ratios.

$$V_{sc} = (\lambda^{-0.5} + 0.025\lambda)(\tau_c A_c + \tau_s A_{st}) \quad (13)$$

Where, λ is the shear span ratio, V_{sc} is the ultimate anti-lateral bearing capacity.

The computed ultimate anti-lateral bearing capacity of SCS walls based on the improved multiaxial strength theory agreed well with the FEM results and the shear test results of 67K specimen. Therefore, the method based on the multi-axial strength theory considering this influence was available for computation purpose of composite structural B-C-W members.

5.2 Results of analysis

The shear span ratio of specimens 67K, 100K and 200K was 0.625 in the shear loading test (Emori 2002). Their axial compression ratios were zero. The experimental ultimate shear strength of these three specimens were compared with the computed ultimate shear strengths using Eq. (13) as reported in Table 4. As can be seen, the computed results are very close to the test results. The

Table 4 Comparison with the experimental data based on the improved multi-axial strength theory

Specimen	Shear span ratio λ	Number of insert plates (n)	Test V_t [MN]	Improved theory V_{sc} [MN]
200K	0.625	0	1.97	1.99
100K	0.625	1	2.04	2.01
67K	0.625	2	2.00	2.03

computed results increased with the increase in the number of insert plates which was consistent with the binding effect of concrete.

6. Conclusions

In this research, a new method to compute the ultimate shear strength of composite structural B-C-W members has been proposed which is based on the multi-axial strength theory. The shear strength of concrete was obtained using concrete failure criterion of Guo-Wang and the shear strength of steel plate was obtained using Von-Mises failure criterion. The limit value of the steel plate slenderness was obtained from the elastic plate theory which could prevent the buckling of the steel plate before yielding. When the CFSB walls are applied in the lower storeys of the tall buildings with strong floors or strong transfer-floors, they would demonstrate obvious shear behavior. For shear test specimens, nonlinear 3-dimensional FEM analyses were performed to simulate the fixed boundary conditions, buckling behavior of surface steel plates, the binding effect of concrete and the interactions between the concrete and steel plates. A validated FE model was developed to carry out further analyses. Based on the shear tests of the specimen 67K and ten FE 3-dimensional models in ABAQUS, a coefficient including the influence of the shear span ratio was added to multi-axial strength theory. In the end, a method to compute the ultimate shear strength of SCS walls was achieved. The main conclusions are as follows:

- (1) The method used to calculate the shear strength of composite structural B-C-W members based on a multi-axial strength theory can be used to compute the ultimate anti-lateral bearing capacity of composite structural B-C-W members with different shear span ratios. The smaller the shear span ratio, the stronger the binding effect of concrete.
- (2) The finite element model of CFSB walls used in this research, considering the influence of initial imperfection has been found to be satisfactory. Through parametric analysis, a coefficient on the shear span ratio was added to the computed formula. The computed results agreed well with the test results.
- (3) The spacing and the strength of the insert plates to induce plate yielding before buckling was determined using elastic plate theory. The buckling length coefficient was suggested to be 0.5.

Acknowledgments

The research is financially supported by the National Natural Science Foundation of China (Grant No. 51708318, 51678322, 51708317 and 51650110509), Ministry of Science and Technology of China (Grant No. 2017YFC0703603), the Taishan Scholar Priority Discipline Talent Group program funded by the Shandong Province, and the first-class discipline project funded by the Education Department of Shandong Province.

References

- ACI 352R-02 (2002), Recommendations for Design of Beam-Column Connections in Monolithic Reinforced Concrete Structures.
- Bradford, M.A., Wright, H.D. and Uy, B. (1998), "Short- and long-term behaviour of axially loaded composite profiled walls", *Proc. Inst. Civ. Eng. Struct. Build.*, **128**(1), 26-37.
- Chen, L., Mahmoud, H., Tong, S.M. and Zhou, Y. (2015), "Seismic behavior of double steel plate-HSC composite walls", *Eng. Struct.*, **102**, 1-12.
- Clubley, S.K., Moy, S.S.J. and Xiao, R.Y. (2003), "Shear strength of steel-concrete-steel composite panels. Part I - testing and numerical modelling", *J. Constr. Steel Res.*, **59**(6), 781-794.
- Dastfan, M. and Driver, R. (2016), "Large-scale test of a modular steel plate shear wall with partially encased composite columns", *J. Struct. Eng.*, **142**(2), 04015142.
- Emori, K. (2002), "Compressive and shear strength of concrete filled steel box wall", *Steel Struct.*, **26**(2), 29-40.
- Guo, Z. and Wang, C. (1991), "Investigation of strength and failure criterion of concrete under multi-axial stresses", *China Civil Eng. J.*, **24**(3), 1-14.
- Hossain, K.M.A., Rafiei, S., Lachemi, M. and Behdinin, K. (2016a), "Structural performance of profiled composite wall under in-plane cyclic loading", *Eng. Struct.*, **110**, 88-104.
- Hossain, K.M.A., Rafiei, S., Lachemi, M., Behdinin, K. and Anwar, M.S. (2016b), "Finite element modeling of impact shear resistance of double skin composite wall", *Thin-Wall. Struct.*, **107**, 101-118.
- Hossain, K.M.A. and Wright, H.D. (2004), "Flexural and shear behaviour of profiled double skin composite elements", *Steel Compos. Struct., Int. J.*, **4**(2), 113-132.
- Huang, Z. and Liew, J.Y.R. (2016a), "Compressive resistance of steel-concrete-steel sandwich composite walls with J-hook connectors", *J. Constr. Steel Res.*, **124**, 142-162.
- Huang, Z. and Liew, J.Y.R. (2016b), "Numerical studies of steel-concrete-steel sandwich walls with J-hook connectors subjected to axial loads", *Steel Compos. Struct., Int. J.*, **21**(3), 461-477.
- Huang, Z. and Liew, J.Y.R. (2016c), "Structural behaviour of steel-concrete-steel sandwich composite wall subjected to compression and end moment", *Thin-Wall. Struct.*, **98**, 592-606.
- Liang, Q.Q., Uy, B., Wright, H.D. and Bradford, M.A. (2003), "Local and post-local buckling of double skin composite panels", *Proceedings of the Institution of Civil Engineers-Structures and Buildings*, **156**(2), 111-119.
- Liang, Q.Q., Uy, B., Wright, H.D. and Bradford, M.A. (2004), "Local buckling of steel plates in double skin composite panels under biaxial compression and shear", *J. Struct. Eng.-Asce*, **130**(3), 443-451.
- Liew, J.Y.R., Yan, J.B. and Huang, Z.Y. (2017), "Steel-concrete-steel sandwich composite structures-recent innovations", *J. Constr. Steel Res.*, **130**, 202-221.
- Link, R.A. and Elwi, A.E. (2004), "Composite concrete -steel plate walls: analysis and behavior", *J. Struct. Eng.-Asce*, **121**(2), 260-271.
- Pant, D.R., Montgomery, M. and Christopoulos, C. (2017), "Analytical Study on the Dynamic Properties of Viscoelastically Coupled Shear Walls in High-Rise Buildings", *J. Eng. Mech.*, **143**(8), 04017047.
- Rabbat, B.G. and Russell, H.G. (1985), "Friction coefficient of steel on concrete or grout", *J. Struct. Eng.*, **111**(3), 505-515.
- Rafiei, S., Hossain, K.M.A., Lachemi, M., Behdinin, K. and Anwar, M.S. (2013), "Finite element modeling of double skin profiled composite shear wall system under in-plane loadings", *Eng. Struct.*, **56**, 46-57.
- Rafiei, S., Hossain, K.M.A., Lachemi, M. and Behdinin, K. (2015), "Profiled sandwich composite wall with high performance concrete subjected to monotonic shear", *J. Constr. Steel Res.*, **107**, 124-136.
- Rahai, A. and Hatami, F. (2009), "Evaluation of composite shear wall behavior under cyclic loadings", *J. Constr. Steel Res.*, **65**(7), 1528-1537.
- Uy, B., Wright, H.D. and Bradford, M.A. (2001), "Strength of profiled composite walls subjected to axial and bending loads", *Proc. Inst. Civ. Eng. Struct. Build.*, **146**(2), 129-139.
- Vecchio, F.J. and McQuade, I. (2011), "Towards improved modeling of steel-concrete composite wall elements", *Nucl. Eng. Des.*, **241**(8), 2629-2642.
- Wang, B., Jiang, H. and Lu, X. (2017a), "Seismic performance of steel plate reinforced concrete shear wall and its application in China Mainland", *J. Constr. Steel Res.*, **131**, 132-143.
- Wang, M., Borello, D.J. and Fahnstock, L.A. (2017b), "Boundary frame contribution in coupled and uncoupled steel plate shear walls", *Earthq. Eng. Struct. Dyn.*, **46**(14), 2355-2380.
- Zhao, Q.H. and Astaneh-Asl, A. (2004), "Cyclic behavior of traditional and innovative composite shear walls", *J. Struct. Eng.-Asce*, **130**(2), 271-284.
- Zhou, D., Liu, L. and Zhu, L. (2016), "Lateral load-carrying capacity analyses of composite shear walls with double steel plates and filled concrete with binding bars", *J. Central South Univ.*, **23**(8), 2083-2091.

DL